

# Functionalized Zeolitic Materials with Photocatalytic Properties

Maria Ignat,<sup>a\*</sup> Laurentia M. Revenco,<sup>a</sup> Adina R. Pascaru,<sup>a</sup> and  
Eveline Popovici<sup>a</sup>

<sup>a</sup> *Laboratory of Materials Chemistry, Department of Chemistry, "Al.I. Cuza" University Iasi, 11 Carol I Bd, Iasi 700506, Romania*

**Abstract:** Zeolite chemistry is still a viably research area with a large palette of uses, among them a photocatalytic topic is very interesting. Photocatalysis over semiconductor oxide is initiated by the absorption of a photon with energy equal to or greater than the band gap of semiconductor, producing electron-hole (e<sup>-</sup>/h<sup>+</sup>) pairs. It is important to prevent electron-hole recombination before a designated chemical reaction occurs on the semiconductor surface. Having recognized that charge separation is a major problem, numerous efforts have been attempted to improve its photocatalytic activity: metal oxide deposition, doping, surface chelation, coupling of two semiconductors.

**Keywords:** clinoptilolite, titanium oxide nanoparticles, photocatalysis.

## Introduction

Zeolites are hydrated aluminosilicates of the alkaline and alkaline-

---

\* PhD Maria Ignat, tel: +40 232 201135, fax: +40 232 201313, e-mail: maria.rudei@chem.uaic.ro

earth metals. Approximately 40 natural zeolites have been identified over the past 200 years, the most common of which are analcime, chabazite, clinoptilolite, erionite, ferrierite, heulandite, laumontite, mordenite, and phillipsite. They are used in a broad field of applications and are commercially valuable because of their unique ion-exchange, molecular sieving, and catalytic properties. A schematic palette of zeolite uses is presented in Figure 1. Due to their ion exchange capability they can act as water softeners or be used for the removal of pollutants, and their well defined cavities allow size-selective reactions, for example in catalysis.<sup>1</sup> Zeolites are also being used for cooling application, like cooling beverages.<sup>2</sup> It is possible to accommodate photoactive guests within the cavities created by the rigid framework. The photoactive guests can be an organic photosensitizer, an inorganic semiconductor or a combination of both. The combination of a zeolite host and photoactive sites renders solid photocatalysts in which the high surface area and the adsorbent capacity provided by zeolites cooperate to increase the efficiency of the photocatalytic process.

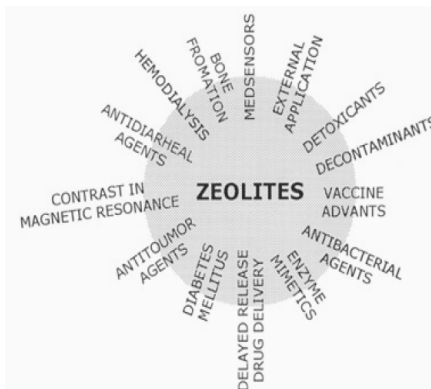


**Figure1.** The palette of zeolite uses.

Photocatalytic oxidation is viewed as an attractive option to be an

alternative waste treatment. Photocatalytic oxidation is an oxidation process that could stimulate chemical reaction with the help from certain catalysts in the presence of UV radiation.

Semiconductors such as  $\text{TiO}_2$ ,  $\text{Fe}_2\text{O}_3$ ,  $\text{ZnO}$ ,  $\text{ZnS}$ ,  $\text{CdS}$  and  $\text{WO}_3$  have been known to possess photocatalytic character. Among them, titanium dioxide ( $\text{TiO}_2$ ) is the most widely used as inorganic catalyst for photocatalytic oxidation process, more for its activeness, great stability and non-toxic character. The photocatalyst, titanium dioxide, is a wide bandgap (3.2 eV) semiconductor, corresponding to radiation in the near UV range. Upon the absorption of this UV energy,  $\text{TiO}_2$  particles will form a paired electron ( $e^-$ ) and hole ( $h^+$ ), in the conduction band and valence band. The positive hole is apparently able to oxidize a water molecule to hydroxyl radical. The hydroxyl radical, in turn, is a powerful oxidant. The oxidation of organic contaminants seems to be mediated by a series of reactions initiated by hydroxyl radical on the  $\text{TiO}_2$  surface. For the photo-oxidation reaction to occur, both  $\text{TiO}_2$  and a UV light source are necessary.<sup>3</sup>

Besides  $\text{TiO}_2$ , molecular sieves, or better known as zeolites are also known as remarkable catalysts. Our study is focused on the extension of the clinoptilolite properties in view of solving some critical environmental problems such as wastewater pollution.<sup>4,5</sup> Heterogeneous photocatalysis has received increasing attention over two decades for purifying a great variety of environmental pollutants in water and air.<sup>5-7</sup> However, the development of a practical water treatment system relative to the photocatalytic oxidation has not yet been successfully achieved.

In this work, clinoptilolite was selected as the catalyst support. Clinoptilolite is of particular interest due their versatile structural features

for the encapsulation of photoactive guests and their related studies. We have been extensively exploring the research area in which clinoptilolite can be used as a host material for accommodating inorganic guests such as metal and semiconductor clusters. The chosen probe molecule was methylene blue, which was a common dye in chemical and processing industries. The objective of the present work was to examine the selected metal oxide ( $\text{TiO}_2$ ) supported on clinoptilolite.

### **Experimental**

As the support of nano-oxides semiconductors, the hydrogen form of clinoptilolite, obtained by ultrasound assisted acid treatment of clinoptilolite from Chilioara Romania, was employed.

Prior to the metal oxide precursor impregnation, it is required to remove the present water in the zeolite framework, to avoid the titanium tetraisopropoxide hydrolysis.

Titanium oxide deposition of clinoptilolite was accomplished in the following way: 1 g of clinoptilolite was dispersed into an alcoholic solution of metal precursors. Clinoptilolite in metal precursor ethanolic solution was then subjected to ultrasonic sound at 50 °C, irradiating with 20 kHz ultrasonic waves at 600 W output power. After 1 hour irradiation, the precipitate was dried at 80 °C over night. Calcination was performed in static air at 400 °C for 4h with a rate flow of 2 °C/min.

The photocatalytic activity of the samples (0.1 g of photocatalyst powder) was tested for the decomposition of Methylene Blue in aqueous solution (300 mL with initial concentration,  $C_0 = 20 \text{ mg/L}$ ). The photocatalytic reactions were taken place in a reactor that consists of two parts: a 400 ml Quartz glass bottle and a 150 W medium pressure Hg lamp

that was parallel to the Quartz glass bottle. In all experiments, the reaction temperature was kept at  $25 \pm 2$  °C. Prior to irradiation, the suspension was magnetically stirred in a dark for 30 minutes in order to establish the adsorption – desorption equilibrium between the catalyst surface and the dye. Then the suspension containing MB and photocatalyst were irradiated under the UV light for 40 minutes and the photocatalytic reaction timing was started. At given time intervals (10 minutes), analytical samples were taken from the reaction suspension, centrifuged at 4000 rpm for 2 minutes. Then the filtrate was analyzed by measuring the concentration of the MB dye in aqueous solution at 665 nm on a UV–visible spectrophotometer (Shimadzu, Japan).

X-ray diffractograms were recorded on a PANalytical X'Pert PRO MPD diffractometer applying monochromatized CuK $\alpha$  radiation. Measurements were done in the 2 $\theta$  mode using a bracket sample holder with a scanning speed of 0.04°/4s continuous mode.

Porosity and surface area studies were performed on a NOVA 2200e system using nitrogen as the adsorbate at liquid nitrogen temperature (-196°C). All the samples were outgassed under vacuum, for 6 hours at 25°C before adsorption measurements. The surface area was calculated using the BET method in the range of relative pressure 0.05-0.35. Pore volume was calculated at the relative pressure of 0.95. Pore sizes distributions were calculated from the adsorption branches of the N<sub>2</sub> adsorption isotherms using the Barrett-Joyner-Halenda BJH model.

UV–Vis diffuse reflectance spectroscopy measurements were carried out using a Shimadzu, Japan spectrophotometer equipped with an integrating sphere attachment. The analysis range was from 200 to 800 nm,

and MgO was used as a reflectance standard.

## Results and discussions

**Structural properties** To reveal the interaction between the TiO<sub>2</sub>, SnO<sub>2</sub>, TiO<sub>2</sub> and the clinoptilolite, the crystal structures of the raw Clinoptilolite and the semiconductor metal oxide loaded clinoptilolite were measured, as shown in Figure 2. According to the XRD pattern shown in Figure 2, the zeolitic matrix is identified as clinoptilolite and its characteristic peaks were recognized ( $2\theta = 11.28^\circ, 22.38^\circ, 22.58^\circ, 30.8^\circ$ ).<sup>8</sup> Clinoptilolite was the major crystalline phase detected on the X-ray diffraction pattern. XRD peaks of clinoptilolite sample were found to be in good agreement with the data of clinoptilolite. In addition to zeolitic and aluminosilicate phases, quartz, cristobalite, and K-feldspar in minor quantities were also detectable in X-ray diffraction patterns.

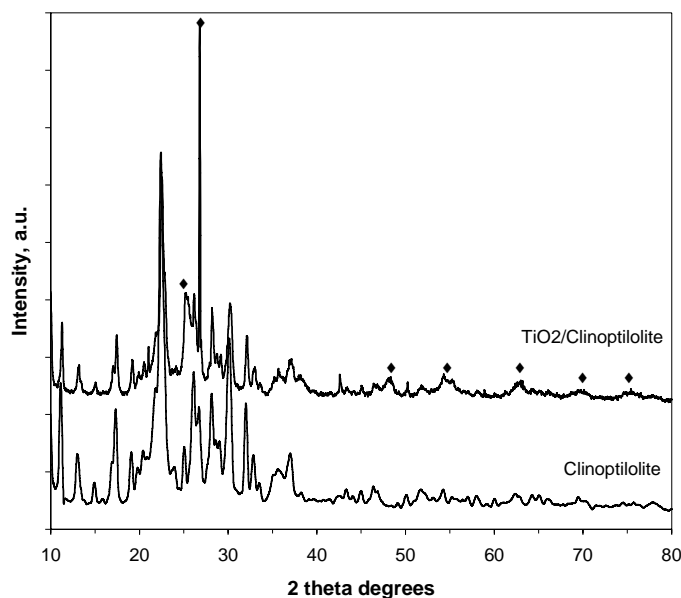


**Figure 2.** XRD patterns of clinoptilolite and TiO<sub>2</sub>-modified clinoptilolite.

Other minerals such as feldspat ( $2\theta = 24.8^\circ, 28.8^\circ$ ) and alpha-quartz (reflection at  $2\theta = 26.68^\circ$ ) were identified in the natural clinoptilolite. It is clear that the XRD pattern of the composite consists with the raw clinoptilolite very well, and it implies that the frame structure of zeolite after metal oxide loading has not been destroyed.

XRD pattern of the  $\text{TiO}_2$ /clinoptilolite powder shows strong diffraction peaks around  $2\theta = 25^\circ, 48^\circ$ , and  $55^\circ$  which are characteristic of anatase-type  $\text{TiO}_2$  (JCPDS 21-1272). On the other hand, the XRD spectrum shows the presence of rutile phase also. The crystallite size of mesoporous titania was estimated from line broadening of the [101] diffraction peak using Debye-Scherrer's equation:

$$D_{hkl} = \frac{0.89\lambda}{B \cos\theta}$$

where,  $\lambda$  is equal to 1.54056 Å, the wavelength for Cu-K $\alpha_1$  radiation, B is the width of the peak at an intensity equal to half the maximum intensity in radians, and  $\theta$  is the diffracted angle at maximum intensity and the grain size was found to be in the range of 7.8 nm.

***TiO<sub>2</sub> bonding possibility*** Infrared spectroscopy yields valuable information concerning the framework of the support and the local metals bonding environment in the obtained nanocomposites. The DRIFT spectra were measured, shown in Figure 3. A new absorption band is found in the DRIFT spectra of  $\text{TiO}_2$ -clinoptilolite comparing with the raw one. The band covers a range from 945 to 905  $\text{cm}^{-1}$  corresponding to the stretching vibration of Ti-O-Si and Ti-O-Al, which is similar to the results from Liu et al.<sup>9</sup> As known, the infrared ray ranging from 400 to 350  $\text{cm}^{-1}$  is mostly reflecting the bond torsions. When the  $\text{TiO}_2$  are combined with clinoptilolite

via Ti–O–Si or Ti–O–Al, the torsions of Ti–O– are restricted by the solid surface bonding. Thus, the energy of the torsion vibration of such bonds becomes weaker. Based on these results, we conclude that during the synthesis process a certain amount of TiO<sub>2</sub> has reacted with the surface –OH of raw clinoptilolite, and created the new bonds like Ti–O–Si and Ti–O–Al. The bond stress is strong enough to keep the TiO<sub>2</sub> caught on the clinoptilolite during the photocatalytic degradation process.

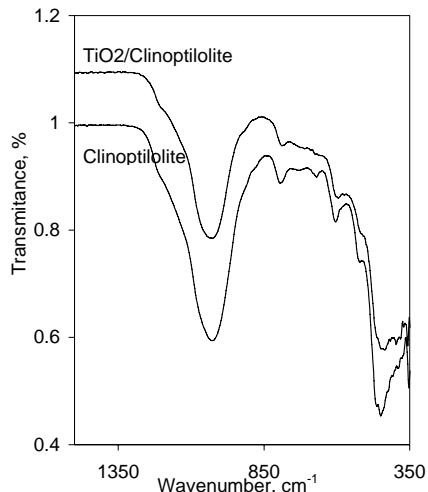


**Figure 3.** FT-IR spectra of raw Clinoptilolite and TiO<sub>2</sub>/Clinoptilolite.

**Textural properties** The textural characteristics were evaluated using conventional nitrogen adsorption–desorption procedure. All materials displayed isotherms of type IV with a distinct hysteresis loop, as it can be seen in Figure 4.

The natural clinoptilolite allows for the presence of a small amount of impurities, especially clays, quartz and amorphous glassy material. This is confirmed by the H3 shape of the hysteresis loop with an inception point at around  $P/P_0 = 0.7$ . The impediment for N<sub>2</sub> to penetrate into the



ultramicropores causes that low pressure hysteresis be absent in this material.

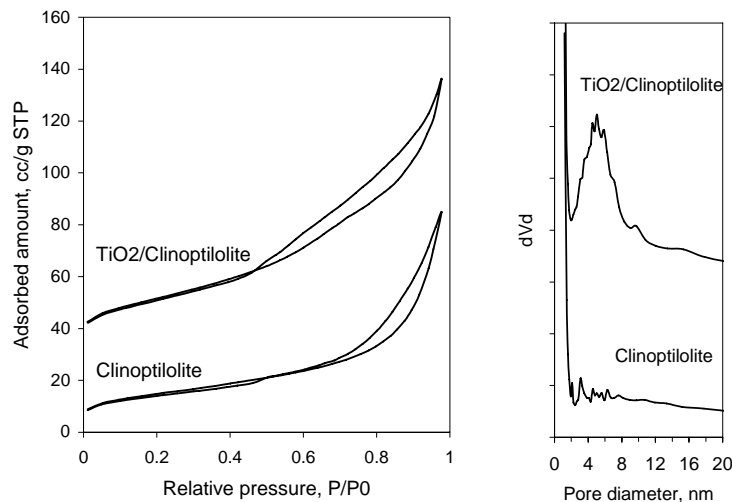


**Figure 4.** The N<sub>2</sub> adsorption-desorption isotherms at 77K (a) and pore size distributions from adsorption branches of raw Clinoptilolite and TiO<sub>2</sub>/Clinoptilolite.

The loaded clinoptilolite isotherm presents a wide and opened hysteresis loop that extends from the 0.7 to 0.45  $P/P_0$  (Figure 5). In the case of raw clinoptilolite, the adsorption data reveals the pore diameter of 3.09 nm (near the border between microporous and mesoporous IUPAC domain), total pores volume about 0.13cm<sup>3</sup>/g and a surface area of 46 m<sup>2</sup>/g that stress the microporous character of clinoptilolite sample.

After titanium oxide loading and thermal treatment at 400 °C, the adsorption data (Table 1) reveal a number of structural changes as an increase of surface area, pore volume and formation of new mesopores.

These new structural future may be explained by the titanium oxide deposition on the clinoptilolite surface, process accompanied by pores obstruction and film deposition on the surface.

**Table 1.** Textural properties and catalytic results of the raw and titanium loaded clinoptilolite.

Sample	$S_{\text{BET}}$ , (m <sup>2</sup> /g)	TPV (cc/g)	Dp (nm)	%adsorption	%photocatalysis
C	46.36	0.13	3.09	33	76
CT	77.1	0.51	5.03	29	98

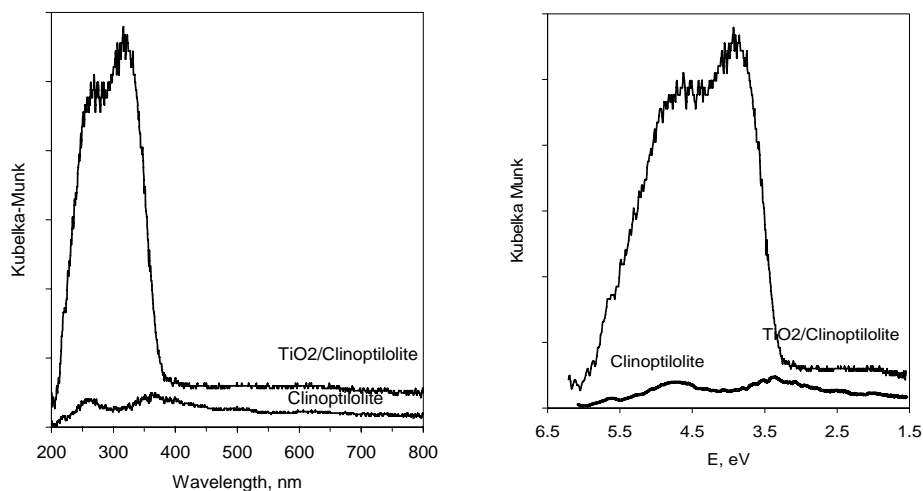


**Figure 5.** Diffuse Reflectance UV-vis spectra for the raw and modified clinoptilolite with titanium oxide.

**Optical properties** The UV-Vis spectra of clinoptilolite and TiO<sub>2</sub>/clinoptilolite are shown in Figure 5. The spectra clearly exhibit the changes in the absorbance edges corresponding to the energy band gap of TiO<sub>2</sub> (3.58 eV). For the TiO<sub>2</sub>/Clinoptilolite sample, an increment in the absorption edge corresponding to TiO<sub>2</sub> is observed. This behavior indicates that the composite has been formed. As revealed in the figure, the band in

the range of 240–250 nm is attributed to a charge transfer of the tetrahedral titanium sites between  $O^{2-}$  and the central Ti(IV) atoms, while octahedral Ti was reported appear at around 260–330 nm.<sup>10</sup>

**The photocatalytic activity** The evolution of the MB concentration as a function of the photoreaction time with catalysts is presented in Fig. 6. Their photocatalytic activity shows an exponential decrement of the MB concentration with respect to time; thus, for correct data processing, the Langmuir-Hinshelwood model for a reaction of first order and for heterogeneous photocatalytic reactions was applied.<sup>11</sup>

As shown in the Figure 6, the photocatalytic efficiency of the studied samples increases with titanium oxide loading. As was expected, the clinoptilolite host-matrix has no photocatalytic activity. In the case of nanocomposite, the enhancement in the photocatalytic activity may come from the hetero-junctions between coupled titanium oxide – clinoptilolite.

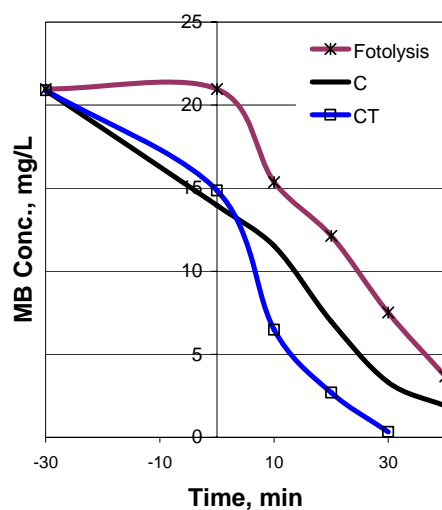


**Figure 6.** Photodegradation of MB solution in UV irradiated clinoptilolite samples.

As a consequence of hetero-junctions TiO<sub>2</sub>-clinoptilolite contribution, the photoactive ·OH (hydroxyl radicals) generated on the semiconductor surface, during irradiation, are easily transferred onto the surface of zeolite. That means the organic pollutants, which have already been adsorbed on the non-photoactive clinoptilolite, have chances to be degraded on the clinoptilolite surface, resulting in the enhancement of the photodegradation performance of TiO<sub>2</sub>/Clinoptilolite.

### **Conclusions**

It was possible to make the synthesis of the TiO<sub>2</sub>/Clinoptilolite by simple impregnation method and a thermal treatment. According to the characterization results, the UV-Vis spectra confirmed the formation of the TiO<sub>2</sub> nanoparticles in the clinoptilolite framework; the XRD results indicate that the TiO<sub>2</sub> is crystalline. The unique and fascinating properties of clinoptilolite involving transition metal oxides present on the zeolitic frameworks have opened new possibilities for many applications, not only in catalysis but also for various photochemical processes. The raw clinoptilolite present photocatalytic activity in the decomposition of MB, but the TiO<sub>2</sub>/Clinoptilolite composite resulted more efficient in the MB photodecomposition. The photodecomposition grade is high, and is probably due to the increase of the band gap energy of the catalyst.

The study has demonstrated the photocatalytic efficiency of the synthesized composites. The presence of the structure created by metal oxide deposition has helped in trapping the organics present in the dye solution.

**References**

1. Weitkamp, J., Raichle, A., and Traa, Y., *Appl. Cat. A*, **222**, 277 (2001).
2. US Patent # 4,924,676, *Zeolite/Water Adsorption Cooling/Heating*, Peter MAIER-LAXHUBER, *et al.*
3. Corma, A., Davis, M., Fornes, V., Alfaro, G., Lobo, R., and Orchilles, V., *Catalysis*, **167**, 438 (1997).
4. Armbruster, T., Galarnau, A., Di Renzo, F., Fajula, F., and Vedin, J. (Editors), *Zeolites and Mesoporous at the Dawn of the 21<sup>st</sup> Century*, *Studies in Surface and Catalysis*, **175**, 13-17 (2001).
5. Popovici, E., Burtica, G., Pode, R., Bedeleian, I., and Calb, I., *Romanian volcanic tuffs exploitation in environmental protection*, *Proceedings of the NATO Advanced research workshop on the application of natural microporous materials for environmental technology*, Smolenice Castle, Slovakia, 345 (1998).
6. Kwon, S., Fan, M., and Yang, H., *Critical Reviews in Environmental Science and Technology*, **38**, 197 (2008).
7. Doula, M., Ioannou, A., and Dimirkou, A., *J. Colloid Interface Sci.*, **245**, 237 (2002).
8. Nikazar, M., Gholivand, K., and Mahanpoor, K., *J. Chin. Chem. Soc.*, **54**, 1261 (2007).
9. Liu, X., Iu, K. K., and Thomas, J. K., *J. Chem. Soc., Faraday Trans.* **89**, 1861 (1993).
10. Nur, H., Hau, N. Y., Misnon, I. I., Hamdan, H., and Muhid, M. N. M., *Materials Lett.*, **60**, 2274 (2006).

11. Hernandez, A., Maya, L., Sanchez-Mora, E., and Sanchez, E.M., *J. Sol-Gel Sci. Technol.*, **42**, 71 (2007).